Spectroscopic and computational studies of $[OsCl_5(NO)]^{3-}$ and $[RuCl_5(NO)]^{3-}$ donors in AgCl

R. S. Eachus, R. C. Baetzold, and Th. D. Pawlik

Imaging Research and Advanced Development, Eastman Kodak Company, Rochester, New York 14650-2021

O. G. Poluektov and J. Schmidt

Huygens Laboratorium, University of Leiden, P.O. Box 9504, 2300 RA, Leiden, The Netherlands

(Received 6 August 1998; revised manuscript received 2 October 1998)

Information about the structure and performance of two metal nitrosyl dopant complexes in irradiated silver chloride powders has been obtained. Experiment and theory suggest that both $[OsCl_5(NO)]^{2-}$ and $[RuCl_5(NO)]^{2-}$ are incorporated substitutionally into AgCl with their ligands intact. Charge compensation is provided by three proximal silver ion vacancies ($=V$). Optimal geometries for the resultant $[MCl_5(NO)]^{2-} \cdot 3V$ centers ($M=$ Ru or Os) have been determined by calculation, with the configuration $(011)(0\bar{1}1)(002)$ being slightly preferred for both metals. The incorporation of these nitrosyls into AgCl introduces midgap vacant levels so that they function as ionized donor centers. Electron trapping results in a series of structural relaxations involving both the dopant and the lattice. The initial deep donor centers produced by trapping are overcompensated structures, $[MCl_5(NO)]^{3-} \cdot 3V$. These centers have been studied by electron paramagnetic resonance spectroscopy at 9, 35, and 94 GHz, and by electron-nuclear double resonance spectroscopy at 9 GHz. Secondary deep donor centers with the formula $[MCl_5(NO)]^{3-} \cdot 2V$ result from vacancy diffusion at 120–140 K. Kinetic experiments show that $[OsCl_5(NO)]^{3-} \cdot 2V$ centers decay with an effective lifetime of about 550 s at 300 K, although it takes more than 4×10^4 s to completely bleach these donors at this temperature. The ruthenium complex has proved to be even more stable. Results described in this paper emphasize the importance of charge compensation and structural relaxations in dopant-related carrier trapping processes. [S0163-1829(99)06013-0]

I. INTRODUCTION

Transition metal (TM) complexes that act as ionized donors are frequently used to control the electronic properties of the microscopic silver halide crystals (or *grains*) employed in photographic imaging. Such dopants can limit reciprocity effects, enhance image contrast, and reduce recombination inefficiencies.[1] The ionized donor may simply act as a shallow (Coulomb) center, or it may deeply trap an electron in its frontier molecular orbital. In the past, practical dopants were usually hexacoordinate complexes with halide ligands, although X^- replacement by H_2O occasionally proved valuable.[2] More advanced doping protocols have exploited the surprisingly high solubility of complexes with bulky, charged ligands in AgX. A wide range of new imaging materials are emerging in which the AgX grains contain, for example, pseudohalide TM complexes like $[Ru(CN)_6]^{4-}$,[3] or TM complexes with organic ligands.[4] The ability of the cubic silver halides to substitutionally accommodate high concentrations of complexes with substantial lattice mismatch is providing many new doping opportunities for these substrates.

This paper describes a study of silver chloride microcrystals doped with $[OsCl_5(NO)]^{2-}$, a complex in which the divalent metal ion has a low spin $5d^6$ electronic configuration and the nitrosyl ligand carries a formal charge of $+1$. Analyses for elemental osmium by ion-coupled plasma mass spectrometry suggest that this dopant might be incorporated into AgCl by coprecipitation from aqueous solution. A more definite conclusion cannot be drawn, however, since such data do not verify the dopant's inclusion with the nitrosyl

ligand intact. Furthermore, they do not reveal its microscopic structure in the AgCl lattice, i.e., if it is dispersed homogeneously or segregated as occlusions. Fortunately, $[OsCl_5(NO)]^{2-}$ has proved to be a potent trap for photoelectrons in this material and structural information on the resultant paramagnetic donor center can be obtained from a combination of multifrequency electron paramagnetic resonance (EPR) and 9.4 GHz electron-nuclear double resonance (ENDOR) measurements. It has been helpful to compare the spectroscopic results obtained from $[OsCl_5(NO)]^{3-}$ with the limited information published for its ruthenium analogue[5] and the data reported here. In order to analyze and assign the experimental data, it was necessary to perform advanced calculations of structure and energy. This combination of experimental and theoretical methodologies revealed an important relaxation process that makes the nitrosyl complexes some of the deepest donor centers found so far in AgCl.

II. EXPERIMENTAL

A. Materials

Because both nitrosyl dopants decomposed at high temperatures and exhibited long-term solution instabilities, we could not grow single-crystal samples for these studies. Thus experiments were confined to AgCl powders, most of which were prepared by conventional precipitation methods as uniform dispersions in aqueous gelatin. Precipitation in aqueous gelatin ensured that, in any one sample, the crystals were cubic and of uniform size (± 0.01 μm). One sample of $[OsCl_5(NO)]^{2-}$-doped AgCl was prepared using polyvinyl

TABLE I. Total vacancy binding energies (ΣBE/eV) calculated for various configurations of $[M\text{Cl}_5(\text{NO})]^{n-}$ centers in AgCl. The NO ligand lies along the z axis near (001).

Number of Vacancies	Vacancy Position(s)	ΣBE/eV			
		$M=\text{Os},$ $n=2$	$M=\text{Os},$ $n=3$	$M=\text{Ru},$ $n=2$	$M=\text{Ru},$ $n=3$
1	(002)	1.44	-	1.67	-
	(00$\bar{2}$)	0.88	0.57	0.86	0.60
	(110)	1.16	0.66	1.16	0.64
	(011)	1.60	0.90	1.49	0.89
2	(002)(00$\bar{2}$)	2.29	-	2.54	-
	(011)(0$\bar{1}$1)	2.91	1.59	2.63	1.55
	(200)($\bar{2}$00)	1.78	1.00	1.73	1.17
	(110)($\bar{1}\bar{1}$0)	2.19	1.18	2.10	1.17
3	(011)(0$\bar{1}$1)(002)	3.56	1.66	3.40	1.80
	(011)(0$\bar{1}$1)(10$\bar{1}$)	3.54	1.76	3.34	1.79

alcohol in place of gelatin. This peptizer proved less effective at maintaining a small grain size distribution and controlling morphology. The nitrosyl dopants were added as aqueous solutions during precipitation. In most cases the nominal dopant concentration was 25 molar parts per million. Dopant location was also an experimental variable. For EPR and ENDOR studies, the amount of gelatin peptizer was minimized by aqueous dilution and centrifugation cycles performed at 40 °C. This procedure leaves traces of the peptizer bound to the AgCl microcrystals. The resultant powders were dried in air following an acetone wash, and stored at 4 °C.

B. EPR and ENDOR experiments

Photo-EPR spectra at 9 GHz and 10–300 K were obtained with a Bruker ESP-300E spectrometer, and were analyzed using a combination of the programs WIN-EPR© and SimFonia© (Bruker Instruments, Inc.). *In situ* irradiations were performed with the output of a 200 W super pressure Hg/Xe light source passing through a combination of a $\frac{1}{8}$ m monochromator and interference and long-pass filters. EPR measurements at 35 GHz and 80–300 K were made on a Varian E-12 spectrometer. Kinetic measurements were also made on this spectrometer using an isochronal thermal pulse technique. EPR experiments at 94 GHz and 2 K were performed on a home-built pulsed spectrometer described elsewhere.[6] ENDOR measurements were performed at 9 GHz and 12 K on a modified Bruker ER-200D spectrometer.

C. Calculation methods

The calculational methods employed here have been previously described.[7] Two separate calculations were performed. The preferred arrangements and binding energies of silver ion vacancies ($=V$) to the dopant were determined by classical atomistic simulation procedures using the General Utilities Lattice Program (GULP).[8] The electronic properties of the dopant-vacancy complex were then determined by quantum-mechanical methods. The latter methods treated the complex by Hartree-Fock and density functional[9] procedures

and considered the effects of the polarizable silver halide lattice. Its total energy including lattice polarization was computed, allowing the determination of ionization potentials and electron affinities. Basis sets were derived from previous functions[10] and the CADPAC code was used for the *ab initio* calculations.[11] It is difficult to assess the absolute accuracy of the various calculations, since there are no experimental vacancy binding energies, electron affinities, or structural data available for the complexes in silver halides. Thus we emphasize trends. In this regard, we have studied various basis sets and compared the results from Hartree-Fock and density-functional theory. The trends are fully consistent.

III. RESULTS

A. Dopant incorporation

We employed atomistic simulation methods in order to determine the most favorable structures for the $[M\text{Cl}_5(\text{NO})]^{2-}$ ($M=\text{Ru}$ or Os) centers in AgCl. Anticipating the results of photochemical experiments to be described in Sec. III C, structures for the corresponding $[M\text{Cl}_5(\text{NO})]^{3-}$ deep donor centers were also addressed. It was found that stable lattices could be achieved when these complexes replaced $(\text{AgCl}_6)^{5-}$. In the case of $[\text{OsCl}_5(\text{NO})]^{2-}$, the equilibrium Os-Cl bond lengths were calculated to be 2.40 Å, which is less than the Ag-Cl distance of 2.75 Å. The Os-N≡O distance was 3.29 Å, slightly longer than the Ag-Cl distance, but overall this dopant fitted rather well into the space normally occupied by $(\text{AgCl}_6)^{5-}$. Similar results were found for $[\text{RuCl}_5(\text{NO})]^{2-}$.

Frenkel defects on the cation sublattice are the primary form of point lattice disorder in AgCl at $T \leqslant 298$ K. Thus, in the absence of surface effects, charge compensation for the $[M\text{Cl}_5(\text{NO})]^{2-}$ complexes is achieved solely through the creation of three silver ion vacancies per dopant center. Vacancy binding energies calculated for both dopants are presented in Table I, where data for the corresponding $[M\text{Cl}_5(\text{NO})]^{3-}$ donors are also included. M is at (000) and

the NO ligand lies along the z axis near (001). These data represent the energy to remove a vacancy from a lattice position next to M to a remote part of the crystal. We see that for $[OsCl_5(NO)]^{2-}$, the optimum geometry has a single vacancy bound by 1.6 eV next to the NO ligand at (011). For two vacancies, the combination of positions $(001)(0\bar{1}1)$ is strongly preferred. The second vacancy is bound by 1.31 eV, which, although large, represents a reduction from the value calculated for the first vacancy. The third vacancy compensating this dopant is bound by >0.6 eV at either the (002) or $(10\bar{1})$ positions.

As in the case of the Os complex, calculations indicate that a single vacancy or a vacancy pair are preferably bound at positions next to the NO ligand of $[RuCl_5(NO)]^{2-}$ in AgCl. In contrast to the situation for $M=Os$, however, the first vacancy prefers (002). The combination of $(011)(0\bar{1}1)$ is again optimum for the pair, and is a natural precursor to the preferred geometry of the center with three vacancies, i.e., $(001)(0\bar{1}1)(002)$. The vacancy binding energies calculated for the $[MCl_5(NO)]^{2-}$ centers in AgCl are so large that, in the materials employed in this study, we expect that all of the nitrosyl complexes will tend towards full local compensation at $T \leq 298$ K.

For the $[MCl_5(NO)]^{3-}$ donors produced by electron trapping, the maximum first vacancy binding energies are reduced to about 0.9 eV at (011). For two vacancies, the axially opposed combination $(011)(0\bar{1}1)$ is preferred for both metals. Calculations also suggest that overcompensated donor centers (i.e., those with three vacancies) are unlikely at temperatures where point defects are mobile in AgCl ($T \geq 140$ K), since binding energies for the extra vacancies are ≤ 0.25 eV.

B. Calculations of structure and energy

We have performed embedded quantum-mechanical calculations of structure and energy for the $[MCl_5(NO)]^{2-}$ dopants and their corresponding donor centers in AgCl. The number and geometrical arrangement of vacancies were varied in these calculations. For both dopants, the most favored vacancy configurations gave M-N=O bond angles of 180° prior to electron trapping. However, when an electron becomes deeply trapped, the M-N=O bond angle bends away from 180° and the zigzag configuration shown in Fig. 1 is frequently adopted. For the most stable donor geometries considered here, the bent configurations are 1–2 eV more stable than their linear analogs. Values calculated for the equilibrium distortion angles of selected examples are included in Table II, where we introduce the shorthand notation $M^\bullet nV$ to denote donors with bound silver ion vacancies. The symbol $^\bullet$ represents an electron deeply trapped by the MnV ionized donor complex.

Note that a strongly distorted zigzag geometry is generally maintained for the donor, whether or not it has associated vacancies. The linear $(011)(0\bar{1}1)(002)$ configuration predicted for Os$^\bullet 3V$ is the only exception. From the data in Table II, we see that the most stable geometries of Os$^\bullet 3V$ and Os$^\bullet 2V$ are considerably less distorted than those of their Ru analogs. Bond bending provides an efficient relaxation mechanism by which to dissipate the electron trapping en-
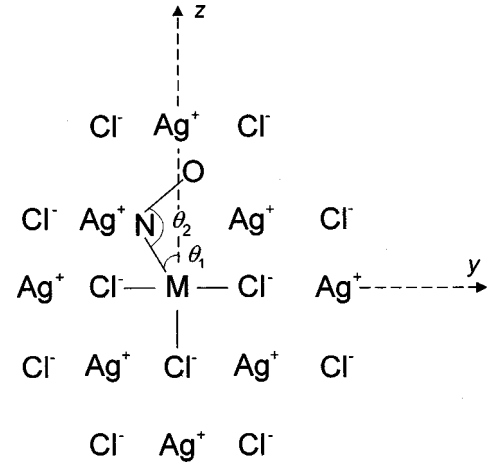

FIG. 1. Projection in yz of the substitutional $[MCl_5(NO)]^{3-}$ center in AgCl (M=Ru, Os) showing the zigzag structure frequently adopted following electron trapping. Values for the equilibrium distortion angles θ_1 and θ_2, as functions of M and the number of associated silver ion vacancies, are included in Table II.

ergy, and introduces a substantial activation barrier to thermal ionization. This is a major reason for the donor's stability. By these arguments, Ru$^\bullet 3V$ and Ru$^\bullet 2V$ are expected to be longer-lived electron traps than their Os counterparts, consistent with experiment (see Sec. III C and Ref. 5).

In the course of these calculations, we examined in detail several possible orientations of the M-N=O bonds for $[RuCl_5(NO)]^{3-}$ in the presence of vacancies at the favored (011) and $(0\bar{1}1)$ positions. This was accomplished by allowing the NO ligand to relax with different degrees of freedom. We considered several orientations of the bent M-N=O moiety with respect to its nearest lattice ions and vacancies. The total energies of the optimized geometries were so close to each other (± 0.09 eV) that it was not possible to choose a preferred orientation. Thus we only calculated data for the zigzag geometry with N displaced in the [110] direction and O displaced along $[\bar{1}\bar{1}0]$. This structure, which offers the greatest separation between the bent NO ligand and its nearest crystal ions, should be favored from a steric point of view.

TABLE II. Equilibrium bond angles ($\theta_i/°$) calculated by the Hartree-Fock (ROHF) method for selected vacancy geometries of $[MCl_5(NO)]^{3-}$ trapped electron centers in AgCl (Ref. 8).

Center	Vacancy Position	θ_1	θ_2
Ru$^\bullet 0V$	-	4.8	158.1
Ru$^\bullet 1V$	(002)	a	a
Ru$^\bullet 2V$	$(011)(0\bar{1}1)$	5.5	142.5
Ru$^\bullet 3V$	$(011)(0\bar{1}1)(002)$	6.3	145.5
Os$^\bullet 0V$	-	5.2	166.1
Os$^\bullet 2V$	$(011)(0\bar{1}1)$	6.3	157.3
Os$^\bullet 3V$	$(011)(0\bar{1}1)(002)$	0.0	180.0
	$(011)(0\bar{1}1)(10\bar{1})$	4.4	148.1

^{a}Data omitted because the Ru-N bond was felt to be unrealistically elongated in the AgCl matrix during calculation.

TABLE III. Electron affinities (EA/eV) calculated by the Hartree-Fock (ROHF) method for $[MCl_5(NO)]^{2-}$ dopants (M = Ru, Os) in AgCl.

Center	Vacancy Position(s)	EA	
		Linear	Bent
Ru0V	-	a	7.70
Ru1V	(002)	b	b
Ru2V	(011)(0$\bar{1}$1)	5.47	7.23
Ru3V	(011)(0$\bar{1}$1)(002)	7.85	8.04
Ru3V^c	(011)(0$\bar{1}$1)(002)	5.22	7.03
Os0V	-	6.45	6.51
Os2V	(011)(0$\bar{1}$1)	6.28	6.42
Os3V	(011)(0$\bar{1}$1)(002)	6.56	6.56[d]
	(011)(0$\bar{1}$1)(10$\bar{1}$)	5.42	5.57

[a]SCF calculations did not converge.

[b]Data omitted because the Ru-N bond unrealistically elongated in the AgCl matrix during calculation.

[c]Values calculated using internuclear distances for the Ru2V complex.

[d]Bent structure relaxes to linear within our accuracy limits.

In order to assess their carrier trapping properties, electron affinities were calculated for several experimentally relevant complexes of $[RuCl_5(NO)]^{2-}$ and $[OsCl_5(NO)]^{2-}$ with silver ion vacancies embedded in AgCl. The results are presented in Table III. Here we have considered the equilibrium, bent M-N≡O structures, as well as the corresponding equilibrium structures if the M-N≡O are not allowed to bend. Unfortunately, the entries for the linear structures are incomplete because of the difficulty in achieving convergence in the self-consistent-field (SCF) calculations. These equilibrium structures were found by performing complete geometry optimizations. In the course of this process, the M-NO bond length in the favored $M3V$ configuration elongated by several tenths of an angstrom relative to the value in $M2V$. This effect was particularly pronounced for the Ru complex (Ru-NO = 2.28 Å). Bond elongation leads to a substantial increase in the calculated electron affinity. Thus, in Table III we also report values for the Ru3V complex calculated at internuclear distances appropriate for the favored geometry of Ru2V. While we consider this bond elongation to be real, it represents an additional relaxation mode that should require activation. At the low temperatures employed in our experiments, the electron affinity calculated for the shorter Ru-NO bond length of Ru2V is probably more realistic.

Fully compensated forms of the dopant before trapping have three associated vacancies, whereas two are required for neutrality after trapping one electron. The largest fractions of Ru and Os dopant centers will be linear $M3V$ complexes prior to actinic exposure, and it is the electron affinities of these centers that determine the trapping properties of these nitrosyls in AgCl. For completeness, other states of compensation have been treated. We feel confident that the general trends observed for the calculated electron affinities are real. Thus, comparisons can be made between the data for Os and Ru complexes in order to predict the relative

carrier trapping properties of these dopants. However, the accuracy of the theoretical electron affinities cannot be determined without appropriate experimental data.

To assess the relative electron trapping propensities of the Os and Ru nitrosyls, the electron affinities calculated for the linear $M3V$ complexes must be compared with the value of 3.6 eV calculated for the conduction band edge of AgCl. Values larger than 3.6 eV are necessary for electron trapping to occur. This condition is met for the linear configurations of Ru3V and Os3V, and the Os donor center should be shallower than its Ru counterpart. We will show later that this is consistent with experiment. Secondary trapping sequences of interest here involve facile relaxations from linear to bent configurations of the $M3V$ centers. The calculations show that bending causes a substantial increase in the electron affinity of the Ru complex, further enhancing the stability of the donor center.

Density-functional calculations were run on several of the $[RuCl_5(NO)]^{n-}$ complexes embedded in AgCl for comparison to the Hartree-Fock results. The trends in the results of the two calculations were very similar, although some numerical differences were noted. Once again, the electron affinity increases upon bending, a relaxation that yields similar zigzag structures to those predicted by Hartree-Fock calculations.

Table IV shows the unpaired electron populations distributed on various atoms calculated according to the Mulliken procedure. Data for the M·0V structures are included to show that the effect of association with silver ion vacancies is a minor perturbation. When M = Ru, the unpaired electron density is always confined primarily to the NO ligand. The linear Os·0V and Os·2V complexes have substantial unpaired electron density on the metal, but much of this is transferred to NO upon bending. The Os·3V complex has the odd electron on NO in both configurations.

Simple molecular-orbital theory may be used in order to understand the interactions between the frontier orbitals involved in the unpaired electron's redistribution in Os·2V and Os·2V upon Os-N≡O bond bending. We are concerned here with the π^* molecular orbitals of NO and the occupied valence d orbitals of the metal. In each of the linear geometries, the level ordering is as shown in Fig. 2(a) where $5d_{z^2}$ is the semioccupied frontier orbital. When the NO ligand lies strictly along z, interactions between $5d_{z^2}$, $5d_{x^2-y^2}$, or $5d_{xy}$ and the nitrosyl π^* orbitals are zero by symmetry. The $5d_{xz}$ and $5d_{yz}$ orbitals interact with the π^* orbitals in the manner sketched in Fig. 2(b). The π^* orbitals are destabilized by this interaction because they lie above both $5d_{xz}$ and $5d_{yz}$. When the Os-N≡O bond bends, weak interactions between $5d_{z^2}$, $5d_{x^2-y^2}$, $5d_{xy}$, and the π^* orbitals become allowed. The dominant effect, however, is a decrease in the overlap between π^* and $5d_{xz}$ and $5d_{yz}$ [Fig. 2(c)]. As a result, the π^* orbitals fall below $5d_{z^2}$, as shown in Fig. 2(d). For Os·3V and Os·2V, the combination of vacancies in the yz plane and bond bending splits the π^* levels producing semioccupied molecular orbitals derived primarily from N and O $2p_x$ orbitals. In the case of Os·2V, the same effect is achieved by bond bending alone. These are the dominant interactions in this simple molecular orbital description. This picture is consistent with the increase in electron affinity and repopulation of N and O orbitals observed in the Hartree-

TABLE IV. Unpaired electron populations calculated for $[MCl_5(NO)]^{3-}$ donors in AgCl (M = Os or Ru) using Hartree-Fock (ROHF) methods.

Donor	Vacancy Positions	Electron Populations			
		M	N	O	Cl
Ru˙$0V$, linear	-	0.00	0.70	0.29	0.01
Ru˙$0V$, bent	-	0.03	0.69	0.27	0.01
Ru˙$2V$, linear	$(011)(0\bar{1}1)$	0.02	0.67	0.31	0.00
Ru˙$2V$, bent	$(011)(0\bar{1}1)$	0.03	0.67	0.29	0.01
Ru˙$3V$, linear	$(011)(0\bar{1}1)(002)$	0.01	0.62	0.37	0.00
Ru˙$3V$, bent	$(011)(0\bar{1}1)(002)$	0.05	0.59	0.36	0.00
Os˙$0V$, linear	-	0.82	0.00	0.00	0.18
Os˙$0V$, bent	-	0.11	0.64	0.23	0.02
Os˙$2V$, linear	$(011)(0\bar{1}1)$	0.88	0.02	0.00	0.10
Os˙$2V$, bent	$(011)(0\bar{1}1)$	0.07	0.68	0.26	0.00
Os˙$3V$, linear[a]	$(011)(0\bar{1}1)(002)$	0.01	0.63	0.35	0.01
Os˙$3V$, linear	$(011)(0\bar{1}1)(10\bar{1})$	0.06	0.68	0.26	0.00
Os˙$3V$, bent	$(011)(0\bar{1}1)(10\bar{1})$	0.06	0.65	0.27	0.02

[a]According to calculation, the bent configuration of Os˙$3V$ relaxes back to the more stable linear configuration.

Fock calculations. In the case of the Ru complexes, the π^* molecular orbital is populated in both linear and bent configurations. This is because the frontier d orbitals of Ru lie lower in energy than those of Os. Thus, there is a larger energy separation between the NO π^* and the metal d orbitals causing less destabilization for the linear geometry. This drives the π^* levels below $4d_{z^2}$ in the linear geometry producing a level structure like that in Fig. 2(d).
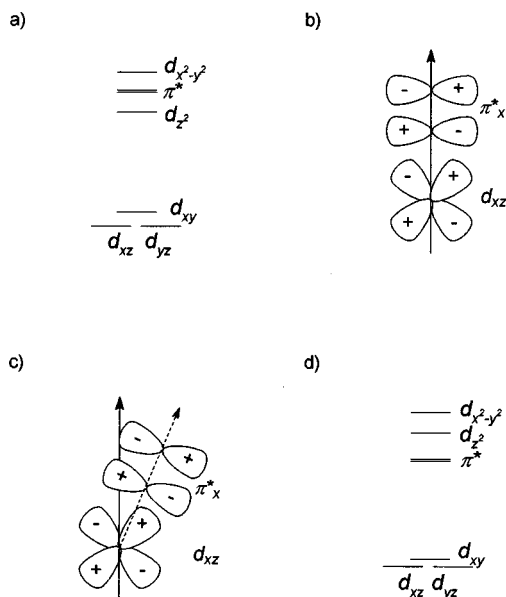

FIG. 2. (a) Energy level scheme for linear —Os-N≡O. The —Os-N≡O axis is z. (b) The dominant metal-ligand interaction is shown for one of the $t_{2g}-\pi^*$ degenerate components. Here, the strong overlap destabilizes π_x^*. (c) Bond bending weakens this interaction. (d) Bending —Os-N≡O causes the ordering of the π^* and $5d_{z^2}$ levels to change because of the weaker $t_{2g}-\pi^*$ interaction. For —Ru-N≡O, the π^* lie below $4d_{z^2}$ in both linear and bent configurations.

This simple molecular orbital theory approach has been applied previously to bonding analysis in various organometallic complexes.[12] Of course, in our situation the complex is incorporated into an inorganic crystal and can have various arrangements of bound vacancies. The presence of these associated point defects will perturb the orbital energy levels through electrostatic effects and, thus, necessitates treatments by embedded self-consistent methods. Indeed, there is often a close balance between bent and linear configurations, and the favored structure can be determined by the actual vacancy configuration. This effect apparently explains the linear structure preferred for Os3V with vacancies at $(011)(0\bar{1}1)(002)$ versus the bent arrangement favored for $(011)(0\bar{1}1)(10\bar{1})$—see Table II. The zigzag structure found in our Hartree-Fock and density-functional calculations is in part due to the steric requirements imposed by the crystal lattice.

C. Photo-EPR and ENDOR studies of $[OsCl_5(NO)]^{2-}$-doped AgCl emulsions

Figure 3 shows an EPR spectrum obtained at 9.3 GHz and 10 K from a 0.38 μm cubic AgCl sample doped with 25 ppm of $[OsCl_5(NO)]^{2-}$ following its exposure to subband gap light between 400 and 440 nm. No EPR signals were detected before exposure or after irradiation at wavelengths longer than 460 nm. There are two paramagnetic centers in about equal abundance contributing to this spectrum. The signal at lower field originates from the self-trapped hole (STH), a tetragonally elongated $(AgCl_6)^{4-}$ acceptor whose EPR spectrum is distinctive and well documented.[13] The second signal will be assigned here to an $[OsCl_5(NO)]^{3-}$ donor. It is difficult to determine the symmetry of this center from Fig. 3 because of spectral overlap in the region around 335 mT. Calculations predict full local compensation by three bound vacancies for the $[OsCl_5(NO)]^{2-}$ precursor, with a
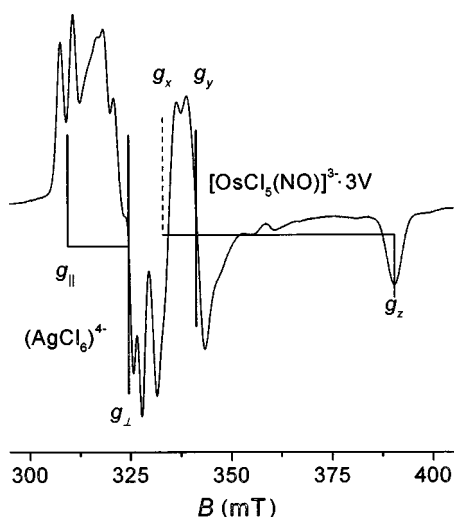
FIG. 3. EPR spectrum obtained at 9.3 GHz and 10 K from a 0.38 μm cubic AgCl sample doped at 25 ppm with $[OsCl_5(NO)]^{2-}$. Spectrum measured after irradiation with 400–440 nm light at 10 K.

$(011)(0\bar{1}1)(002)$ arrangement being only slightly preferred energetically over $(011)(0\bar{1}1)(10\bar{1})$. The low temperature employed in this experiment will limit vacancy rearrangement following electron trapping. Thus, this donor is likely to have the overcompensated structure Os$^{\bullet}$3V, with bound silver ion vacancies at (011), $(0\bar{1}1)$, and either (002) or $(10\bar{1})$. Only a single type of Os$^{\bullet}$3V center was produced by irradiation, implying that one of these vacancy configurations is, in fact, favored. Unfortunately, as will become clear later, we cannot determine this configuration experimentally. At this time, we assume it to be $(011)(0\bar{1}1)(002)$, the minimum energy structure predicted by theory (see Table I).

Irradiation with above-band gap light ($\lambda = 365$ nm) produced Os$^{\bullet}$3V by electron trapping from the conduction band edge. Its yield in this experiment closely matched those from exposures to subband gap light, but the production of the STH was substantially better at this shorter wavelength, as judged by the integrated areas under the EPR spectra. This can be explained if $[OsCl_5(NO)]^{2-}$ traps more than one electron during high intensity, above-band gap exposures, a conclusion consistent with the results of kinetic measurements described later. A low spin $[OsCl_5(NO)]^{4-}$ double donor center would be diamagnetic and remain undetected in the EPR experiment.

To determine the symmetry of Os$^{\bullet}$3V and to better derive its magnetic resonance parameters, electron spin-echo-detected EPR spectra were measured at 94 GHz and 2 K for a range of UV-irradiated samples. Figure 4 shows a spectrum obtained from a 0.35 μm cubic AgCl sample containing a nominal 100 ppm of $[OsCl_5(NO)]^{2-}$ following its exposure to 310–320 nm light. At 94 GHz, the absorption signals from the STH are well separated from those of Os$^{\bullet}$3V. There was a slight loss in resolution of the spectrum when going to 94 GHz believed to be the result of g-strain broadening. The Os$^{\bullet}$3V donor is now clearly seen to have orthorhombic symmetry with $g_z = 1.7030$ and $g_y = 1.9487$. The value determined for g_x (≈ 2.00) is approximate because of overlap with a sharp, weak signal near free spin. Considering g fac-

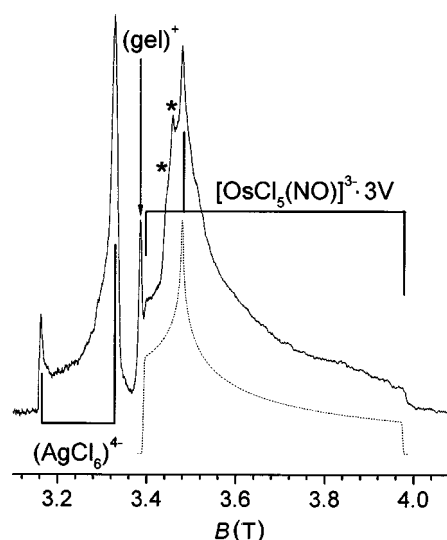FIG. 4. Electron spin-echo-detected EPR spectrum obtained at 94 GHz and 2 K from a 0.35 μm cubic AgCl sample doped at 100 ppm with $[OsCl_5(NO)]^{2-}$. Spectrum measured after exposure to 310–320 nm light at 2 K. The dashed line is a simulation based on the g factors for $[OsCl_5(NO)]^{3-} \cdot 3V$ donors included in Table V. The features marked with asterisks are from an impurity, believed to be $[(H_2O)OsCl_4(NO)]^{2-}$.

tors alone suggests an assignment of this weak signal to the photographic latent image,[1] but it was observed following irradiation at temperatures where interstitial silver ions do not migrate in AgCl. This argues strongly against such an interpretation. It most probably results from radicals in gelatin residues adsorbed to surfaces of the AgCl grains. These radicals could not be generated in $[OsCl_5(NO)]^{2-}$-doped AgCl prepared in polyvinyl alcohol, consistent with this assignment. ENDOR measurements performed on this radical gave a strong matrix-ENDOR signal from electron-nuclear dipole-dipole interactions with distant protons, but showed no hyperfine (HF) or superhyperfine (SHF) lines from interactions with neighboring magnetic nuclides.

UV-irradiated samples of $[OsCl_5(NO)]^{2-}$-doped AgCl were sensitive to long wavelength light at 10 K. Exposure to $\lambda \geq 600$ nm rapidly bleached STH's with no concomitant loss of Os$^{\bullet}$3V donors. The fate of the STH is not known at this time; it was not destroyed by donor-acceptor pair recombination. One possibility is the formation of molecular chlorine[14,15] at surfaces of the AgCl grains following photoexcited hole diffusion. The gelatin radicals were unaffected by red light and continued to obscure the g_x region of the Os$^{\bullet}$3V spectrum. This was not a problem for the sample prepared with polyvinyl alcohol as the peptizer, as is clear from the 9.3 GHz spectrum shown in Fig. 5. This spectrum was analyzed assuming an orthorhombic g matrix with a triplet SHF splitting from a single ^{14}N nucleus resolved at g_x. We performed powder ENDOR measurements on this sample in an attempt to derive the remaining ^{14}N SHF matrix components. A representative spectrum obtained with B_0 at g_y (347.5 mT) is included in Fig. 6. The signal at 14.78 MHz is assigned as a proton matrix-ENDOR feature resulting from electron-nuclear dipole-dipole interactions between Os$^{\bullet}$3V centers at near-surface locations and protons in gelatin or water in the grains' environment. The majority of EN-
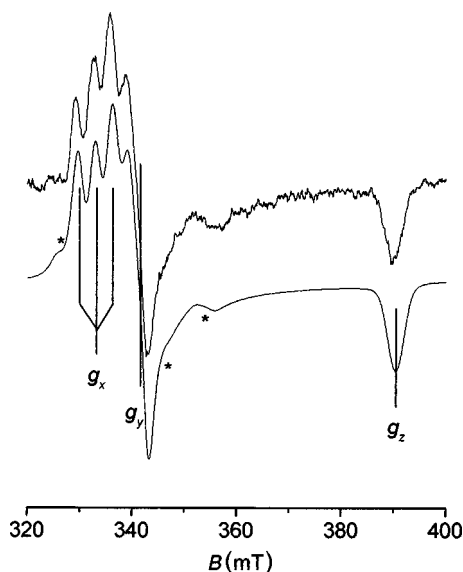
FIG. 5. EPR spectrum obtained at 9.3 GHz and 10 K from a 0.38 μm cubic AgCl sample doped at 25 ppm with $[OsCl_5(NO)]^{2-}$. Spectrum measured after first irradiating with 365 nm light at 10 K and then bleaching $(AgCl_6)^{4-}$ centers with red light. The lower spectrum is a simulation based on the parameters determined for $[OsCl_5(NO)]^{3-} \cdot 3V$ donors and included in Table V. The asterisks indicate features assigned as ^{189}Os hyperfine structure at g_y.

DOR lines appearing between 5 and 12 MHz are assigned as hyperfine features from interactions with second-shell or more distant ^{107}Ag $(I=\frac{1}{2})$ and ^{109}Ag $(I=\frac{1}{2})$ nuclides. This interpretation is consistent with the observed line intensities and the ratio of the derived ^{107}Ag and ^{109}Ag hyperfine coupling constants. The four signals observed in the frequency range 15–22 MHz are most reasonably assigned to interactions between the unpaired electron and the ^{14}N nuclide of
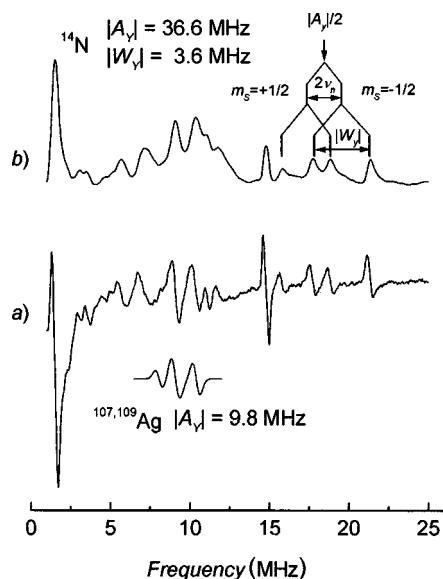

FIG. 6. Powder ENDOR spectrum measured at 9.43 GHz and 12 K from a 0.38 μm cubic AgCl sample doped at 100 ppm with $[OsCl_5(NO)]^{2-}$. Spectrum measured after irradiating sample with 365 nm light at 87 K. (a) Spectrum measured with 350 KHz FM modulation. (b) Integration of spectrum shown in (a). See text for justifications of the spectral assignments.

the nitrosyl ligand. This spectrum is that expected for a situation in which (i) the hyperfine coupling constant is much larger than ν_n, the Larmor frequency for ^{14}N, and (ii) there is a finite nuclear quadrupole interaction. To first order, the signals are centered at a frequency of $|A_y/2|$ and are split into a primary doublet separated by $2\nu_n$ (=2.14 MHz at 347.5 mT), as shown in Fig. 6. The nuclear quadrupole interaction further splits these $m_s = \pm\frac{1}{2}$ lines into doublets separated by W_y, the quadrupole interaction parameter along y. The slight angular dependences of these features could be followed when B_0 was in the range 340–352 mT, but it proved impossible to measure ^{14}N ENDOR with B_0 at g_z (390 mT), preventing a precise determination of $|A_z|$. Finally, EPR spectra at 9.3 and 94 GHz were simulated for comparison to experiment using linewidths as fitting parameters. The result at 9.3 GHz is included in Fig. 5. For completeness, this simulation included a ^{189}Os $(I=\frac{3}{2}$, 16.1% natural abundance) HF interaction of 8.47 mT at g_y and set an upper limit of 1 mT for the ^{14}N $|A_z|$ value.

When a fresh sample of $[OsCl_5(NO)]^{2-}$-doped AgCl was exposed to subband gap light at 10 K and then annealed above 40 K, the STH began to diffuse and decay. As in the red-light bleaching experiments, its decay was not the result of donor-acceptor pair recombination with Os$^{\bullet}3V$, the latter being stable up to 120 K. Between 40 and 60 K, two paramagnetic centers resulted from loss of the acceptor. The first gave a broad, asymmetric EPR signal near 320 mT. This signal, commonly observed in studies of AgCl grains doped with deep electron traps, is assigned as holes transiently trapped by silver ions at surface or near-surface locations. It will be the subject of a future report. The second product of annealing was additional gelatin radical. The intensity of its isotropic, structureless EPR signal at $g=2.0049$ ($\Delta B=1.6$ mT) increased about tenfold during this treatment. Since it was formed concomitantly with the decay of hole centers in AgCl, it is thought to be a cationic radical. The structure of this species is, as yet, unknown, and so it is labeled as $(gel)^+$ in this report. The oxidant could be $(AgCl_6)^{4-}$, atomic chlorine, or Cl_2.[14]

Continued annealing of the UV-irradiated, gelatin-peptized emulsion to room temperature caused additional changes in the EPR spectrum. Following warming to 200 K and quenching to 10 K, the signals from $(gel)^+$ radicals and Os$^{\bullet}3V$ donors were greatly reduced in intensity (Fig. 7), the latter being replaced by a new spectrum showing a well-resolved triplet splitting on one of its features [Fig. 7(a)]. We assign this spectrum to a second $[OsCl_5(NO)]^{3-}$ center, Os$^{\bullet}2V$, produced by the diffusion of the extra vacancy from Os$^{\bullet}3V$ to a remote lattice site. Based on the results of the binding energy calculations (Table I), a $(011)(0\bar{1}1)$ vacancy geometry is assigned to Os$^{\bullet}2V$. This center was produced in highest yields by subband gap exposures at 250 K, although it was also detected after irradiation at room temperature. If we assume Os$^{\bullet}2V$ is axially symmetric, we cannot account for the relative intensities of the features centered at about 355 and 405 mT [see Fig. 7(b)]. However, if it has rhombic symmetry, an acceptable correlation between calculated and experimental spectra can be achieved [Fig. 7(c)]. Here, g_x was estimated by assuming that the average g factor for Os$^{\bullet}2V$ is equal to that measured for Os$^{\bullet}3V$. A value of g_x
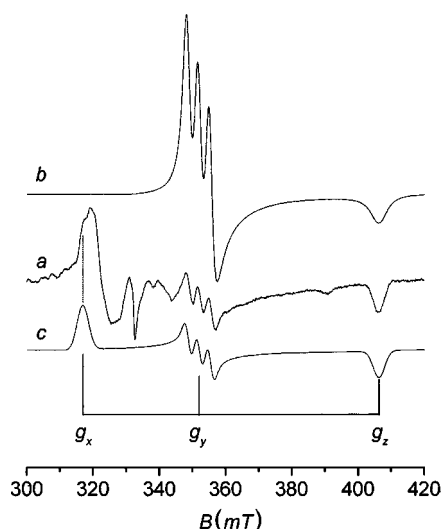
FIG. 7. EPR spectrum measured at 9.3 GHz and 10 K from a 0.40 μm cubic AgCl sample doped at 25 ppm with $[OsCl_5(NO)]^{2-}$. (a) Spectrum measured after irradiation with 365 nm light at 10 K and dark annealing to 200 K. (b) Simulation assuming uniaxial symmetry. (c) Simulation assuming rhombic symmetry. The feature at g_x in (c) is seen as a shoulder at about 318 mT in (a).

$=2.103$ is thus obtained. In fact, features close to this g position were observed at 9.3 and 94 GHz, although there was considerable overlap with other signals at both frequencies. We were unable to measure ENDOR spectra for $Os^{\bullet}2V$ because of its low concentration, large g spread, and short T_1 time. Thus, only the $|A_y|$ component of the ^{14}N SHF matrix is reported with its g factors in Table V.

The $Os^{\bullet}2V$ donors persisted for several hours at 300 K following generation by UV irradiation at 250 K. Their decay could not be followed directly by EPR at this temperature, however, because fast spin relaxation prevented their detection above 50 K. Kinetic data were obtained using an isochronal thermal pulse method in which the relative donor concentration was measured by double integration of the EPR signal obtained at 10 K. The kinetic data obtained for an annealing temperature of 300 K could not be satisfactorily fitted to first order, second order, simple combinations of first and/or second order, or diffusion-controlled[16] kinetics. A

good fit was achieved out to 1.4×10^4 s assuming a logarithmic dependence on decay time. Kinetic data obtained for annealing temperatures between 250 and 310 K were characterized by (i) a surprising temperature independence to the slopes at long times, and (ii) clear evidence for a complex convolution of competitive generation and decay processes at early times. In fact, the concentration of $Os^{\bullet}2V$ increased by as much as 30% in the first few seconds of annealing at 250 K. This behavior can be explained if, once again, we assume that $[OsCl_5(NO)]^{2-}$ acts as a doubly ionized donor in AgCl so that long exposures to band-gap light produce substantial populations of $[OsCl_5(NO)]^{4-}$. This diamagnetic center will have a lower ionization potential than $Os^{\bullet}2V$. It would decay first during annealing, momentarily increasing the concentration of $Os^{\bullet}2V$, as observed experimentally. To facilitate comparisons of dopant behavior, we have estimated an effective lifetime for $Os^{\bullet}2V$ of about 550 s at 300 K; it decayed completely in about 4×10^4 s. A lifetime at 300 K of $\geq 1.6 \times 10^9$ s was reported previously for the corresponding $Ru^{\bullet}2V$ center in AgCl.[5]

We observed no significant effect of grain size on the behavior of $[OsCl_5(NO)]^{2-}$ in AgCl. To assess the dependence on dopant location, a comparison was made between the EPR spectra obtained from two exposed and annealed emulsions to which $[OsCl_5(NO)]^{2-}$ was added in bands. In one, it was confined to a region between 0 and 5% of the grain volume. In the second, a peripheral band between 95 and 100% was doped at the same nominal concentration (Table I). Exposures to 420 nm light at 10 K produced $Os^{\bullet}3V$ donors in both emulsions. These converted to $Os^{\bullet}2V$ donors at 200 K, but a low concentration of a third $[OsCl_5(NO)]^{3-}$ center was detected in grains where the dopant was confined to the perimeter (see Fig. 8). This new center at the near-surface location gave an anisotropic EPR spectrum similar to that of $Os^{\bullet}2V$, but with substantial shifts in g_y and g_z factors. In this case, g_x was clearly resolved at 9.3 GHz [see Fig. 8(b)]. Since it forms only when the dopant is in the space-charge region of the silver halide grain, a region rich in Ag^+ interstitials but deplete of cation vacancies, structures like $Os^{\bullet}1V$ or $Os^{\bullet}0V$ are suggested. The low site symmetry reflected in the anisotropic g matrix favors an assignment to $Os^{\bullet}1V$ and calculation puts the vacancy at

TABLE V. Magnetic resonance data obtained for $[MCl_5(NO)]^{3-}$ centers in cubic AgCl emulsions. $M = Os$ or Ru.

Center	g factors (± 0.0005)			^{14}N Hyperfine Values/mT		
	g_x	g_y	g_z	$|A_x|$	$|A_y|$	$|A_z|$
$Os^{\bullet}3V$	1.9980	1.9487	1.7030	3.28	1.34	$\leq 1^c$
$Os^{\bullet}2V$	2.103^a	1.8900	1.6382	^{b}	3.35	$\leq 1^c$
$Os^{\bullet}nV$ ($n=1$ or 0)	2.128	1.8640	1.6020	^{b}	3.2^d	^{b}
$Ru^{\bullet}3V$	2.0219	2.0219	1.9340	2.5^e	2.5^e	$\leq 1^{c,e}$
$Ru^{\bullet}2V$	2.0230	2.0230	1.9342	2.5^e	2.5^e	$\leq 1^{c,e}$

^{a}Values estimated assuming $g_{av} = 1.888$.
^{b}Not resolved experimentally.
^{c}Estimated from spectral simulation.
^{d}Value ± 0.2 mT.
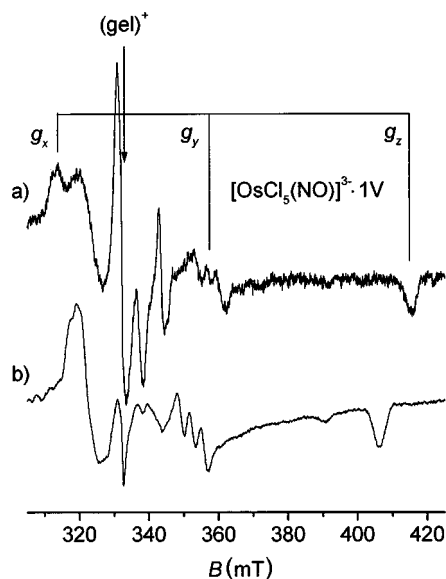^{e}Derived assuming uniaxial symmetry—see Sec. III D for details.

FIG. 8. EPR spectra obtained at 9.3 GHz and 10 K from 0.38 μm cubic AgCl samples doped at 25 ppm with $[OsCl_5(NO)]^{2-}$. Both samples exposed to 420 nm light at 10 K followed by dark anneals to 200 K. In (a), dopant added in peripheral band from 95 to 100% of grain volume. In (b), dopant added from 3.5 to 90% of the grain volume.
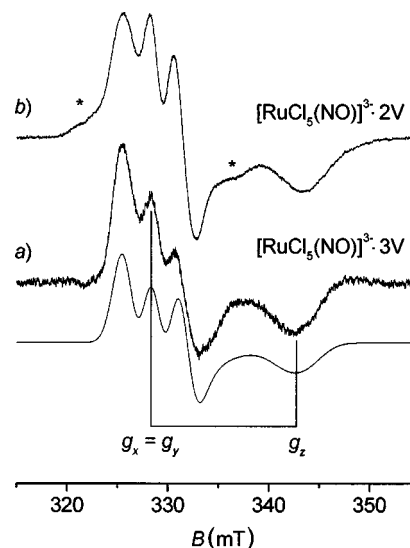

FIG. 9. EPR spectra measured at 9.3 GHz and 10 K from 0.4 μm cubic AgCl grains doped with 25 ppm $[RuCl_5(NO)]^{2-}$. (a) Sample exposed to 540 nm light at 10 K and then bleached with $\lambda \geqslant 650$ nm to eliminate $(AgCl_6)^{4-}$. Spectrum assigned as $[RuCl_5(NO)]^{3-} \cdot 3V$. Lower trace is a simulation based on data in Table V. (b) Sample exposed to 540 nm light at 300 K. Spectrum assigned as $[RuCl_5(NO)]^{3-} \cdot 2V$. Origin of features marked with asterisks is unclear (see text).

(011) (see Table I). This center could only be produced in very low yields, but it was more stable than either Os$^{\bullet}3V$ or Os$^{\bullet}2V$. This is consistent with its additional positive site charge, which will increase its ionization potential and contribute, thereby, to its thermal stability.

D. Photo-EPR studies of $[RuCl_5(NO)]^{2-}$-doped AgCl emulsions

In order to investigate the influence of the TM ion on the photochemistry of nitrosyl-containing AgX dopants, experiments similar to those performed on $[OsCl_5(NO)]^{2-}$-doped AgCl were repeated for its ruthenium analog. Exchanging Ru for Os considerably extended the sensitivity of the doped AgCl grains to subband gap radiation. Substantial yields of two paramagnetic photoproducts could be produced by exposures to light between 420 and 560 nm at 10 K, with traces of these defects resulting from irradiation out as far as 600 nm. One of these centers, the STH, could be bleached by a subsequent exposure to red light ($\lambda > 650$ nm). The spectrum of the remaining photoproduct, a dopant-related donor center, is shown in Fig. 9(a). In this experiment the sample was a 0.40 μm AgCl emulsion doped with 25 ppm of $[RuCl_5(NO)]^{2-}$. This EPR spectrum, measured at 9.3 GHz and 10 K, is believed to originate from a single kind of trapped electron center, although it is difficult to be certain in view of the large linewidths involved. This conclusion was reached because the spectrum did not change in shape with variations in the irradiation wavelength and exposure time, or during thermal annealing treatments by which it was destroyed. It is assigned as the ruthenium analog of Os$^{\bullet}3V$. Theory predicts a $(011)(1\bar{1}1)(002)$ vacancy geometry for Ru$^{\bullet}3V$ (Table I) with a bent Ru-N$=$O bond (Table II) and substantial unpaired electron density on nitrogen (Table IV).

The low-symmetry zigzag configuration predicted for such a structure should result in an orthorhombic g matrix. However, powder EPR spectra obtained at 9.3 GHz and 10 K, and 35.3 GHz and 77 K suggest uniaxial symmetry, and reasonable correlations between simulated and experimental spectra [e.g., Fig. 9(a)] were achieved on this basis with the data included in Table V. A possible explanation is that, above 10 K, Ru$^{\bullet}3V$ undergoes librational relaxation between the two symmetry related zigzag structures predicted by theory. This process might be facilitated by the extra lattice volume afforded through its association with three silver ion vacancies. Further work is in progress to address this issue.

A similar, but not identical 9.3 GHz spectrum was obtained at 10 K after 540 nm irradiation of a fresh sample at room temperature [Fig. 9(b)], or by annealing an emulsion exposed at 10 to 300 K in the dark. By analogy to the results from $[OsCl_5(NO)]^{3-}$, we assign the new spectrum to the neutral species Ru$^{\bullet}2V$. As in the case of the Os donors, the conversion from Ru$^{\bullet}3V$ to Ru$^{\bullet}2V$ occurred in the region of 120–140 K where point defects in AgCl begin to diffuse. The spectrum of Ru$^{\bullet}2V$ again appears to be axial, in contradiction to theoretical predictions. However, it changed substantially and reversibly with temperature, consistent with the occurrence of dynamical relaxation in the range 10–77 K.

There is a small increase in g anisotropy on going from Ru$^{\bullet}3V$ to Ru$^{\bullet}2V$, and a decrease in EPR linewidth, especially at $g_{\perp}$. Furthermore, the spectrum of Ru$^{\bullet}2V$ has two unexplained features: the weak signal on the low-field side of $g_{\perp}$ and the broad shoulder at about 336 mT [marked with asterisks in Fig. 9(b)]. These features were originally thought to be from impurities or decomposition products introduced during doping. They were still observed, however, from samples prepared using carefully purified dopant salts under

conditions designed to minimize their decomposition. An alternative explanation is that they result form a secondary population of Ru$^{\bullet}2V$ donors with a different geometrical arrangement of vacancies. However, this is inconsistent with binding-energy calculations that show a preference for the $(011)(0\bar{1}1)$ geometry of about 0.38 eV. Finally, they might be EPR ''overshoot'' features originating from the Ru$^{\bullet}2V$ donors.[17] These can result when the principal directions of the g and ^{14}N A matrices are noncoincident, a situation that would occur if the Ru-N==O bond is indeed substantially bent.

To date, we have been unable to detect EPR signals that could be assigned to Ru$^{\bullet}1V$ or Ru$^{\bullet}0V$ centers in AgCl grains.

IV. DISCUSSION

A. Electronic structure

Optical-absorption studies have shown that $[\mathrm{OsCl_5(NO)}]^{2-}$ and $[\mathrm{RuCl_5(NO)}]^{2-}$ are stable for several hours in acidified gelatin solutions containing a substantial excess of Cl^-.[18] In this study, such dopant solutions were used within minutes of their preparation. Thus, we assume that the nitrosyls do not decompose during precipitation and that they are incorporated intact into the AgCl grains. Calculations suggest that the replacement of an $(\mathrm{AgCl_6})^{5-}$ lattice unit by an $[M\mathrm{Cl_5(NO)}]^{2-}$ complex is favored, and that the majority of $[M\mathrm{Cl_5(NO)}]^{2-}$ complexes incorporated by precipitation will have three associated silver ion vacancies, especially at low temperatures. For $M=$Os, linear M-N==O structures with vacancies at (001), $(0\bar{1}1)$, and (002), or (011), $(0\bar{1}1)$, and $(10\bar{1})$ should occur in almost equal fractions, and they should have similar electron trapping properties. In practice, however, a single kind of donor center is produced by light exposure suggesting that kinetic processes select only one of these geometrical arrangements at low temperatures. For the purposes of this discussion, we will assume that this is $(011)(0\bar{1}1)(002)$, for which calculation predicts the slightly larger total vacancy binding energy. When $M=$Ru, this vacancy arrangement is also preferred for the linear Ru3V ionized donor.

For the linear Os$^{\bullet}3V$ donor, the electrostatic effect of the two nearest-neighbor vacancies along y will split the degeneracy of the π^*NO orbitals. The ground-state MO will thus comprise of Os $6s$ and $5d_{z^2}$ orbitals hybridized with π_x^* from NO. From simple first-order arguments,[19] the ordering of the g factors will then be $g_z < g_x \approx g_y$, and the nitrogen SHF matrix will have its largest principal value along x. This is consistent with experiment.

An analysis of the EPR and ENDOR data can give a rough estimate of the unpaired electron distribution in Os$^{\bullet}3V$. Ignoring dipole-dipole contributions to the ^{14}N SHF interaction matrix, and assuming uniaxial symmetry for nitrogen, we can set $A_x = A_\parallel = (a_{\mathrm{iso}} + 2b)$ and approximate $A_\perp$ as the average of A_y and $A_z (=a_{\mathrm{iso}} - b)$. The terms have their usual meanings.[20] For unit spin population in the nitrogen $2s$ orbital ($\alpha_{2s}^2 = 1$), a_{iso} is calculated to be 64.62 mT.[21] For unit spin population in the nitrogen $2p$ orbital ($\alpha_{2p}^2 = 1$), $b = 1.981$ mT.[21] We cannot determine the signs of the

principal SHF parameters experimentally, so that all combinations must be considered. Only those with both $A_\parallel$ and $A_\perp$ positive, or $A_\parallel$ positive and $A_\perp$ negative give physically meaningful solutions (i.e., $\alpha_{2s}^2 + \alpha_{2p}^2 \lesssim 1$, $2b > 0$). With both $A_\parallel$ and $A_\perp$ positive, $\alpha_{2s}^2 \approx 0.03$ and $\alpha_{2p}^2 \approx 0.36$, which gives a total nitrogen spin population that is smaller than 0.63, the value calculated by Hartree-Fock methods for the linear configuration of Os$^{\bullet}3V$ (Table IV). Somewhat closer correlation is found assuming $A_\parallel$ positive and $A_\perp$ negative. Then, $\alpha_{2s}^2 \approx 0.005$, $\alpha_{2p}^2 \approx 0.75$. The large p/s ratio derived from this analysis is consistent with the linear structure predicted by theory. Bending of the M-N==O bond would mix substantial nitrogen $2s$ orbital density into the semioccupied MO. Similar analyses of the magnetic-resonance data derived for Os$^{\bullet}2V$ and Os$^{\bullet}nV$ ($n=0$ or 1) donors are confounded by the effects of the increased bond bending predicted by calculation and by the absence of ENDOR data. The substantial structural relaxations of these donors predicted in Table II will result in g and ^{14}N A matrices that have noncoincident principal directions. This means that the largest SHF splittings measured at the g_y positions for Os$^{\bullet}2V$ and Os$^{\bullet}nV$ ($n = 0$ or 1) are unlikely to be principal values of the ^{14}N SHF matrices. There is also the possibility of ''overshoot'' lines[17] in their powder spectra, but the small ^{14}N SHF splittings relative to the experimental linewidths appears to preclude resolution of these extra features.

Similar problems occur for spin population analyses of the data from Ru$^{\bullet}3V$ and Ru$^{\bullet}2V$ because both donors are predicted to have highly distorted structures (Table II). However, the detection of large ^{14}N SHF splittings on ''$g_\perp$'' implies that, in each case, the semioccupied MO has substantial nitrogen $2p$ character, consistent with theory (Table IV).

B. Photochemistry

To understand the photochemistry of $[M\mathrm{Cl_5(NO)}]^{2-}$-doped AgCl grains, it is helpful to construct one-electron energy level models from the combined results of experiment and calculation, as in Fig. 10. On this basis, their sensitivity to subband gap light can be explained by a combination of two processes: (i) a lattice-to-dopant charge transfer transition, and (ii) a concerted mechanism in which an internal d-d transition of the dopant is followed by charge (hole) transfer to the lattice from its excited state. A similar scheme was proposed to explain the behavior of $(\mathrm{RhCl_6})^{3-}$ deep ionized donors in AgCl.[22] In (i), excitation of electrons from the valence band edge to the lowest unoccupied molecular orbitals (LUMO) levels of the dopant generates the $[M\mathrm{Cl_5(NO)}]^{3-}$ deep donor directly; the hole at the valence band edge instantaneously self-traps. The activation energy for hole diffusion in AgCl is about 65 meV,[16] so that the donor-acceptor pairs produced by subband gap light are likely to remain associated at 10 K.

AgCl emulsions doped with $[\mathrm{RuCl_5(NO)}]^{2-}$ proved to be particularly sensitive to light in the region of 550 nm, with dopant induced absorption extending out as far as 600 nm. With (i) as the lowest energy process, this sets the energy for this charge transfer transition at about 2.1 eV. The lowest energy d-d transition for $[\mathrm{RuCl_5(NO)}]^{2-}$ in aqueous solution is at about 568 nm,[23] and this is expected to be only slightly shifted in the AgCl lattice. Thus, the energy of process (ii) is about 2.2 eV. Taking these data into account, and
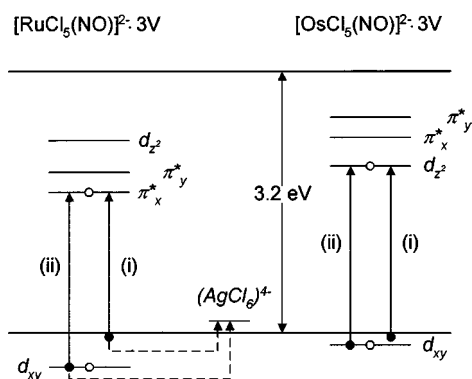
FIG. 10. One-electron energy level models derived from calculated and experimental data, proposed to explain the photochemistry of $[M\mathrm{Cl}_5(\mathrm{NO})]^{2-}$-doped AgCl ($M=\mathrm{Ru}$, Os). (i) Lattice-to-dopant charge-transfer transition. (ii) Concerted charge-transfer process initiated by d-d excitation of dopant complex. The ordering of dopant levels is shown for linear —M-N≡O structures with optimal geometries for the three associated silver ion vacancies. The π^* orbital degeneracy is removed by the two vacancies along the y axis.

assuming a band-gap energy of 3.2 eV, allows us to place π^*_x at about 1.1 eV below the conduction band edge with the dopant's highest occupied molecular orbital (HOMO) at or just below the valence band edge. Consistent with these estimations, there was no evidence of hole trapping by $[\mathrm{RuCl}_5(\mathrm{NO})]^{2-}$ when diffusion of the STH was induced by light or heat. Calculations place the $5d_{z^2}$ LUMO of $[\mathrm{OsCl}_5(\mathrm{NO})]^{2-}$ above the $\pi^*_{x,y}$ levels of $[\mathrm{RuCl}_5(\mathrm{NO})]^{2-}$. This explains the former dopant's lack of sensitivity to visible light beyond 460 nm. The $M^\bullet 3V$ and $M^\bullet 2V$ donor centers of both metals showed no propensity to bleach during exposure to red light ($\lambda \geqslant 650$ nm), conditions that photoionized STH centers. Thus their optical ionization energies must exceed 1.9 eV.

V. CONCLUSIONS

By combining state-of-the-art structural calculations with multifrequency EPR and ENDOR spectroscopic measurements, we have generated detailed models for the structure and performance of two metal nitrosyl dopant complexes in

silver chloride. Our results are consistent with structural models in which the $[M\mathrm{Cl}_5(\mathrm{NO})]^{2-}$, where $M=\mathrm{Ru}$ or Os, are incorporated with their ligands intact into precipitates of AgCl. Substitution for $(\mathrm{AgCl}_6)^{5-}$ is predicted by calculation, with linear M-N≡O bonds in each case. In cubic AgCl grains ranging in size from 0.05 to 0.4 μm, charge compensation is achieved by association of each dopant complex with three silver ion vacancies. The most favorable geometry for $M3V$ appears to be $(001)(0\bar{1}1)(002)$, although other geometries are close in energy. The incorporation of these nitrosyls into AgCl introduces low-lying midgap LUMO levels that facilitate deep electron trapping.

Electron trapping proceeds in a series of steps requiring structural relaxations of both the dopant and the lattice. In the first step, the deep donor center is an overcompensated $[M\mathrm{Cl}_5(\mathrm{NO})]^{3-}\cdot 3V$ structure in which the M-N≡O bond is linear. Electron trapping may cause this bond to bend, and the degree of bending is largest when $M=\mathrm{Ru}$. This lowers the energy of the semioccupied MO associated with the donor center, helping to dissipate the trapping energy. In the second stage, the donor complex is converted to a more stable configuration, $[M\mathrm{Cl}_5(\mathrm{NO})]^{3-}\cdot 2V$, by the diffusion of the excess vacancy to a remote lattice site.

The $[\mathrm{RuCl}_5(\mathrm{NO})]^{3-}\cdot 2V$ donor center has exceptional stability at 300 K, decaying by NO evolution rather than by thermal ionization.[5] Although significantly less stable, its osmium analog is still long lived at room temperature. It decays via a convoluted series of reactions, the exact details of which are still unknown. The process is, however, reversible so that NO ligand loss can be excluded from consideration as a principal decay mechanism. There is indirect experimental evidence that $[\mathrm{OsCl}_5(\mathrm{NO})]^{3-}\cdot 3V$ can trap more than one electron during light exposure.

[1] R. S. Eachus and M. T. Olm, Annu. Rep. Prog. Chem., Sect. C: Phys. Chem. **83**, 3 (1986).

[2] K. Endo and M. Saikawa, J. Photogr. Sci. **38**, 210 (1990).

[3] E. L. Bell, K. J. Reed, and M. T. Olm, U.S. Patent No. 5, 132, 203 (1992).

[4] M. T. Olm, W. G. McDugle, S. A. Puckett, T. Y. Kuromoto, R. S. Eachus, E. L. Bell, and R. D. Wilson, U.S. Patent No. 5,360,719 (1994).

[5] W. G. McDugle, R. S. Eachus, and M. T. Olm, in *Papers Summaries*, 44th Annual Conference of the Society for Photographic Science and Engineering, St. Paul, Minnesota, 1991.

[6] J. A. J. M. Disselhorst, H. van der Meer, O. G. Poluektov, and J. Schmidt, J. Magn. Reson., Ser. A **115**, 183 (1995).

[7] R. C. Baetzold, J. Phys. Chem. B **101**, 1130 (1997).

[8] J. D. Gale, J. Chem. Soc., Faraday Trans. **93**, 629 (1997).

[9] A. D. Becke, Phys. Rev. A **33**, 3098 (1988); C. Lee, W. Yang, and R. G. Parr, Phys. Rev. B **37**, 785 (1988).

[10] Y. Sakai, E. Migoshi, M. Klobukowski, and S. Hunzinaga, J. Comput. Chem. **8**, 226 (1987).

[11] CADPAC: The Cambridge Analytical Derivatives Package, Issue 6, Cambridge, 1995, R. D. Amos, with contributions from I. L. Alberts, J. S. Andrews, S. M. Colwell, N. C. Hardy, D. Jayatilaka, P. I. Knowles, R. Kobayashi, K. E. Laidig, G. Lasming, A. M. Lee, P. E. Maslen, C. W. Murray, J. E. Rice, E. D. Simandiras, A. J. Stone, M. D. Sen, and D. J. Tozer.

[12] R. Hoffmann, M. Chen, M. Elian, A. Rossi, and D. Mingos, Inorg. Chem. **13**, 2466 (1974).

[13] M. Höhne and M. Stasiw, Phys. Status Solidi **25**, K55 (1968); **28**, 247 (1968).

[14] H. Kanzaki and T. Mori, Semicond. Insul. **5**, 401 (1983).

[15] H. Kanzaki and T. Mori, Phys. Rev. B **29**, 3573 (1984).

[16] W. B. Paul, S. Goldenberg, L. Rowan, and L. Slifkin, Cryst. Lattice Defects Amorphous Mater. **15**, 197 (1987).

[17] For further discussions, see F. E. Mabbs and D. Collison, *Electron Paramagnetic Resonance of d Transition Metal Compounds* (Elsevier, Amsterdam, 1992), Chap. 7.

[18] Determined by optical spectroscopy, W. G. McDugle (unpublished).

[19] For example, see P. W. Atkins and M. C. R. Symons, *The Structure of Inorganic Radicals* (Elsevier, Amsterdam, 1967), p. 101.

[20] See for example J. A. Weil, J. R. Bolton, and J. E. Wertz, *Electron Paramagnetic Resonance: Elementary Theory and Practical Applications* (Wiley, New York, 1994).

[21] J. R. Morton and K. F. Preston, J. Magn. Reson. **30**, 577 (1978).

[22] R. S. Eachus and R. E. Graves, J. Chem. Phys. **61**, 2860 (1974).

[23] D. Guenzburger, A. Garnier, and J. Danon, Inorg. Chim. Acta **21**, 119 (1977).